Nov 7th, 12:00 AM - Nov 8th, 12:00 AM

Using Generalized Beam Theory to Assess the Behavior of Curved Thin-Walled Members

Nuno Peres

Rodrigo Goncalves

Dinar Camotim

Wei-Wen Yu International Specialty Conference on Cold-Formed Steel Structures
St. Louis, Missouri, U.S.A., November 7 & 8, 2018

Using Generalized Beam Theory to assess the behavior of curved thin-walled members

Nuno Peres[1], Rodrigo Gonçalves[1] and Dinar Camotim[2]

Abstract

In this work, the first-order behavior of naturally curved thin-walled bars with circular axis, without pre-twist, is assessed with the help of the Generalized Beam Theory (GBT) formulation previously developed by the authors. With respect to the previous work, which dealt with simple cross-sections, the present paper presents a method to obtain the deformation modes for arbitrary flat-walled cross-sections. Despite the complexity involved in this generalization, the standard GBT kinematic assumptions are kept, since they are essential to (i) subdivide the modes in a meaningful way and (ii) reduce the number of DOFs necessary to obtain accurate solutions. It is shown that the curvature of the bar influences significantly the deformation mode shapes. Furthermore, a standard displacement-based finite element (FE) is employed to solve several examples that highlight the peculiar behavior of curved members. For validation and comparison purposes, results obtained using shell FE models are provided. Finally, the superiority of a mixed GBT-based FE format is demonstrated.

1. Introduction

Generalized Beam Theory (GBT) is a thin-walled bar theory incorporating cross-section deformation through the consideration of hierarchical and structurally meaningful cross-section DOFs, the so-called "cross-section deformation modes". GBT was initially proposed and developed by Schardt (1966, 1989), and it is currently well-established as an efficient, versatile, accurate and insightful

[1] CERIS and Departamento de Engenharia Civil, Faculdade de Ciências e Tecnologia, Universidade NOVA de Lisboa, 2829-516 Caparica, Portugal.
[2] CERIS and DECivil, Instituto Superior Técnico, Universidade de Lisboa, Av. Rovisco Pais, 1049-001 Lisbon, Portugal.

approach to assess the structural behavior of thin-walled prismatic bars (e.g., Camotim et al., 2010a, 2010b).

Quite recently, the authors developed, for the first time, a linear GBT formulation for elastic thin-walled bars with circular axis, without pre-twist (Peres et al., 2016). This formulation extends the classic prismatic case while still making it possible to incorporate (or not) the usual GBT strain assumptions. Moreover, it extends the classic theories of Winkler (1868) and Vlasov (1958). Although all types of cross-section deformation modes can be handled, their systematic determination for complex cross sections was not developed, since the so-called "natural Vlasov modes" (complying with Vlasov's assumption) need to be calculated using a complex constraint for curved bars. This paper closes the previous work by proposing a procedure for the calculation of the cross-section deformation modes for members with circular axis and arbitrary flat-walled cross-sections, extending the concepts introduced for the prismatic case in (Gonçalves et al., 2010; 2014; Bebiano et al., 2015). The modes are hierarchized and subdivided using specific kinematic constraints (such as the Vlasov assumption), to keep the usual efficiency of the GBT analyses, namely to ensure that the modal decomposition of the solution provides in-depth insight into the mechanics of the problem under analysis. A set of representative numerical examples is presented, to show the capabilities of the finite element (FE) implementation of the proposed formulation. Moreover, it is demonstrated that a mixed format is more efficient than a standard displacement-based format.

2. First-Order GBT for Members with Circular Axis

For completeness of the paper, the fundamental equations derived in (Peres et al., 2016) are reviewed. Fig. 1 shows the *global* cylindrical (θ, Z, R) and the *local* wall (x, y, z) coordinate systems for an arbitrary curved thin-walled member. The member axis arc-length coordinate X defines the arbitrary cross-section "center" C, lies on the $Z = Z_C$ horizontal plane and has curvature equal to $1/R_C$. For the wall *local* axes, y and z define the mid-line and through-thickness directions, respectively, and x is concentric to X. Moreover, φ is the wall rotation angle.

The standard GBT variable technique is employed for the membrane displacements (u, v, w) along (x, y, z), respectively,

$$u^M = \overline{\boldsymbol{u}}^T(y)\,\boldsymbol{\phi}'(X), \qquad v^M = \overline{\boldsymbol{v}}^T(y)\,\boldsymbol{\phi}(X), \qquad w^M = \overline{\boldsymbol{w}}^T(y)\,\boldsymbol{\phi}(X), \quad (1)$$

where bold letters indicate column vectors, the "bar" vectors contain the deformation mode functions, the $\boldsymbol{\phi}$ vectors collect the corresponding amplitude functions, the commas indicate derivatives (*e.g.*, $f_{,x} = \partial f/\partial x$) and the prime $'$ is used

for a derivative with respect to X. Using small-strains and Kirchhoff's thin-plate assumption, to eliminate plate-like shear locking and write the displacements in terms of the membrane displacements, the strains are given by

$$\boldsymbol{\varepsilon} = \boldsymbol{\varepsilon}^M + \boldsymbol{\varepsilon}^B = \begin{bmatrix} \varepsilon_{xx} \\ \varepsilon_{yy} \\ \gamma_{xy} \end{bmatrix} = \boldsymbol{\Xi}_{\boldsymbol{\varepsilon}} \begin{bmatrix} \boldsymbol{\phi} \\ \boldsymbol{\phi}' \\ \boldsymbol{\phi}'' \end{bmatrix}, \qquad \boldsymbol{\Xi}_{\boldsymbol{\varepsilon}} = \begin{bmatrix} \boldsymbol{\xi}_{11}^T & \mathbf{0} & \boldsymbol{\xi}_{13}^T \\ \boldsymbol{\xi}_{21}^T & \mathbf{0} & \mathbf{0} \\ \mathbf{0} & \boldsymbol{\xi}_{32}^T & \mathbf{0} \end{bmatrix}, \quad (2)$$

$$\boldsymbol{\xi}_{11}^M = \bar{\beta}\left(K_y \overline{\boldsymbol{w}} - K_z \overline{\boldsymbol{v}}\right), \ \boldsymbol{\xi}_{13}^M = \bar{\beta}\overline{\boldsymbol{u}}, \ \boldsymbol{\xi}_{21}^M = \overline{\boldsymbol{v}}_{,y}, \ \boldsymbol{\xi}_{32}^M = \bar{\beta}\overline{\boldsymbol{v}} + \bar{\beta}K_z\overline{\boldsymbol{u}} + \overline{\boldsymbol{u}}_{,y}, \quad (3)$$

$$\boldsymbol{\xi}_{11}^B = -z\bar{\beta}\left(-K_z\overline{\boldsymbol{w}}_{,y} + \bar{\beta}K_y^2\overline{\boldsymbol{w}} - \bar{\beta}K_yK_z\overline{\boldsymbol{v}}\right), \ \boldsymbol{\xi}_{13}^B = -z\bar{\beta}^2\overline{\boldsymbol{w}}, \ \boldsymbol{\xi}_{21}^B = -z\overline{\boldsymbol{w}}_{,yy}, \quad (4)$$

$$\boldsymbol{\xi}_{32}^B = -z\bar{\beta}\left(2\overline{\boldsymbol{w}}_{,y} + 2\bar{\beta}K_z\overline{\boldsymbol{w}} - K_y\overline{\boldsymbol{u}}_{,y} + \bar{\beta}K_y\overline{\boldsymbol{v}} - \bar{\beta}K_yK_z\overline{\boldsymbol{u}}\right), \quad (5)$$

where M/B designate membrane/bending terms, $K_y = \cos\varphi/R_C$, $K_z = -\sin\varphi/R_C$ are the curvatures along the local axes and $\bar{\beta} = R_C/\bar{R}$, where $\bar{R}$ is the mid-line radius.

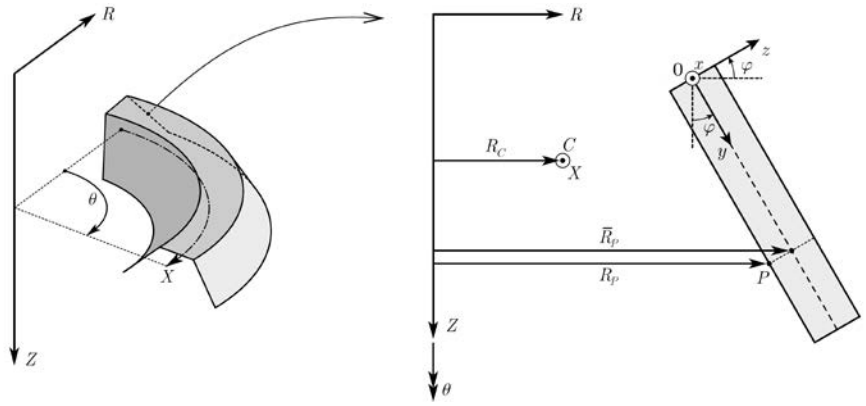

Fig. 1. Global and local (wall) axes for a naturally curved thin-walled member

The homogeneous form of the differential equilibrium equations reads

$$\mathbf{C}\boldsymbol{\phi}'''' - (\mathbf{D} - \mathbf{F} - \mathbf{F}^T)\boldsymbol{\phi}'' + (\mathbf{G} + \mathbf{E} + \mathbf{E}^T + \mathbf{B})\boldsymbol{\phi} = \mathbf{0}, \quad (6)$$

where $\mathbf{D} = \mathbf{D}_1 - \mathbf{D}_2 - \mathbf{D}_2^T$ and the GBT modal matrices read

$$\mathbf{B} = \int_A \frac{E}{1-\nu^2}\frac{R}{R_C}\boldsymbol{\xi}_{21}\boldsymbol{\xi}_{21}^T dA, \qquad \mathbf{C} = \int_A \frac{E}{1-\nu^2}\frac{R}{R_C}\boldsymbol{\xi}_{13}\boldsymbol{\xi}_{13}^T dA, \quad (7)$$

$$\mathbf{D}_1 = \int_A \frac{GR}{R_C}\boldsymbol{\xi}_{32}\boldsymbol{\xi}_{32}^T dA, \qquad \mathbf{D}_2 = \int_A \frac{\nu E}{1-\nu^2}\frac{R}{R_C}\boldsymbol{\xi}_{21}\boldsymbol{\xi}_{13}^T dA, \quad (8)$$

$$\mathbf{E} = \int_A \frac{\nu E}{1-\nu^2}\frac{R}{R_C}\boldsymbol{\xi}_{11}\boldsymbol{\xi}_{21}^T dA, \qquad \mathbf{F} = \int_A \frac{E}{1-\nu^2}\frac{R}{R_C}\boldsymbol{\xi}_{11}\boldsymbol{\xi}_{13}^T dA, \quad (9)$$

$$\mathbf{G} = \int_A \frac{E}{1-\nu^2}\frac{R}{R_C}\boldsymbol{\xi}_{11}\boldsymbol{\xi}_{11}^T dA. \quad (10)$$

In these expressions, A is the cross-section area, E is Young's modulus, ν is Poisson's ratio and G is the shear modulus. If $\varepsilon_{yy}^{M} = 0$ is assumed, the Poisson terms for the membrane strains are eliminated and membrane/bending coupling is eliminated by taking $R/R_C \approx \bar{R}/R_C = 1/\bar{\beta}$. In Peres et al. (2016) the equilibrium equations are also written in terms of stress resultants, and the external load terms and the natural boundary conditions are also given.

3. Cross-section Deformation Modes

For the determination of the deformation modes, the cross-section is discretized using (i) "natural" nodes, automatically located at wall mid-line intersections and free edges, and (ii) "intermediate" nodes, arbitrarily located in the walls, between natural nodes, defining the discretization level. An initial basis for the modes is generated using three DOFs per node: two in-plane displacements (the in-plane rotations are condensed, as in the classic GBT formulations) and one warping. Between nodes, as usual, Hermite cubic functions are employed for $\bar{w}_k$ and linear functions for $\bar{v}_k$ and $\bar{u}_k$. For members with circular axis, linear $\bar{u}_k$ functions can be shown to be consistent with the Vlasov ($\gamma_{xy}^{M} = 0$) and $\varepsilon_{yy}^{M} = 0$ assumptions, which read, from the strain-displacement equations,

$$\bar{v}_{k,y} = 0, \qquad \bar{v}_k = -\frac{\bar{u}_{k,y}}{\bar{\beta}} - K_z \bar{u}_k. \tag{11}$$

It is noted that the latter is significantly more complex to handle than its prismatic member counterpart. However, it is fundamental to subdivide the deformation modes – for open sections it is generally acceptable to consider only the modes with $\gamma_{xy}^{M} = 0$ – and eliminate shear locking. For illustrative purposes, Fig. 2 shows the initial modes for a lipped channel discretized with a single intermediate node in the web, leading to 21 modes.

The final deformation modes are calculated from the initial basis through change of basis operations using the GBT modal matrices and assuming $R/R_C \approx 1/\bar{\beta}$, leading to membrane-bending uncoupling. The following mode sets are defined:

- *Vlasov natural modes*, generated from the natural node warping DOFs and satisfying $\gamma_{xy}^{M} = \varepsilon_{yy}^{M} = 0$. As in the classic GBT, this set is subdivided into (i) distortional and (ii) rigid-body modes (extension, bending and, for open sections, torsion).
- *Local-plate modes*, also satisfying $\gamma_{xy}^{M} = \varepsilon_{yy}^{M} = 0$ but involving essentially plate bending.
- *Shear modes* ($\gamma_{xy}^{M} \neq 0$ and $\varepsilon_{yy}^{M} = 0$), which are subdivided into (i) cell shear flow modes for closed sections (torsion is included), (ii) warping functions of

the Vlasov modes and (iii) additional warping functions. The shear modes generated by the intermediate node DOFs are included in the latter subset.

- *Transverse extension modes*, satisfying $\varepsilon_{yy}^{M} \neq 0$, including the intermediate node DOFs.

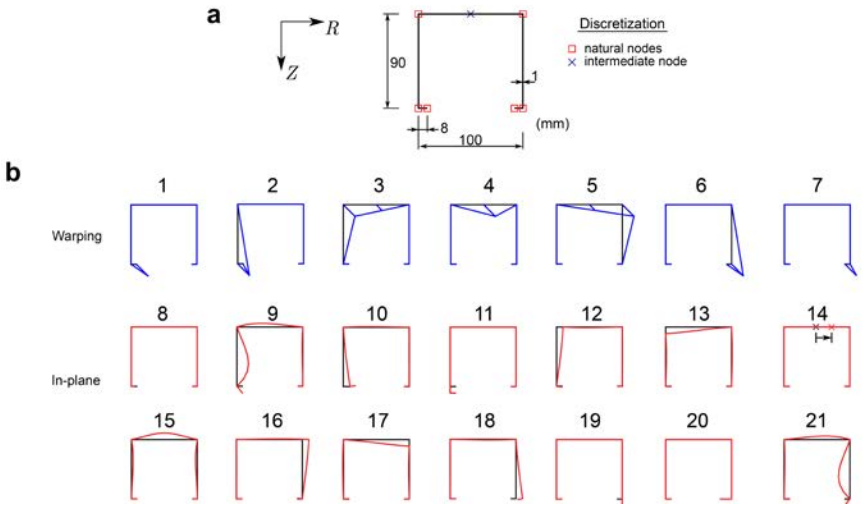

Fig. 2. Lipped channel (a) geometry and discretization, (b) initial deformation modes.

From the strain-displacement relations, it is observed that modes complying with the Vlasov constraint span the nullspace of $\mathbf{D}_1^M$, whereas the null membrane transverse extension modes belong in the nullspace of $\mathbf{B}^M$. Both matrices are necessarily positive semi-definite and one solves

$$(\mathbf{B}^M - \lambda \boldsymbol{I})\boldsymbol{v} = \mathbf{0}, \tag{12}$$

where the $\lambda \neq 0$ eigenvectors define the $\mathbf{B}^M$-orthogonal transverse extension modes. The $\lambda = 0$ eigenvectors satisfy $\varepsilon_{yy}^{M} = 0$ and thus contain the remaining mode sets. One then solves, in the latter space,

$$(\mathbf{D}_1^M - \lambda \boldsymbol{I})\boldsymbol{v} = \mathbf{0}, \tag{13}$$

where the $\lambda = 0$ eigenvectors define a basis for the Vlasov and local-plate modes. These modes are hierarchized as in the procedure proposed by Schardt (1989) for prismatic members, namely by solving

$$\left(\mathbf{B}^M - \lambda(\mathbf{C}^M + \mathbf{C}^B)\right)\boldsymbol{v} = \mathbf{0}, \tag{14}$$

with the $\lambda = 0$ eigenvectors defining the rigid-body mode subspace and the remaining eigenvectors corresponding to the Vlasov distortional and local-plate modes. The rigid-body modes are extracted as in the classic formulations for beams with circular axis (e.g. Dabrowski, 1968): C coincides with the centroid and the first three modes correspond to tangential (mode 1), radial (mode 2) and out-of-plane (mode 3) rigid-body displacements. Using Eq. (6b), it can be shown that mode 3 involves a torsional rotation equal to $-1/R_C$.

The torsion mode for open sections is calculated by working in the 4-D rigid-body mode space and calculating the $\lambda \neq 0$ eigenvector of

$$(\mathbf{D}_1^B - \lambda \mathbf{C}^M)\boldsymbol{v} = \mathbf{0}, \tag{15}$$

since the nullspace of $\mathbf{D}_1^B$ corresponds to $\gamma_{xy}^B = 0$ and matrix $\mathbf{C}^M$ ensures orthogonality of the torsion warping stress resultant with respect to the first three modes. For closed sections, the torsional mode belongs to the shear mode space, as discussed next.

The determination of the shear modes is based on the procedure proposed in (Gonçalves et al., 2014) for the prismatic case. This set is subdivided into: (I) cell shear flow modes, which only exist in closed sections, (II) warping functions of the Vlasov modes and (III) additional warping functions. The II modes are obtained by retaining only the warping functions of the Vlasov natural modes, excluding mode 1 (extension). For the III modes, the orthogonal complement (in the $\mathbf{C}^M$ sense) of the II subset plus mode 1, in the warping mode space, is first obtained. The modes are orthogonalized and hierarchized through

$$(\mathbf{D}_1^M - \lambda \mathbf{C}^M)\boldsymbol{v} = \mathbf{0}. \tag{16}$$

For the I modes, a basis pertaining to independent $\bar{v}$ displacements of the walls is obtained and added to the II and III shear modes, excluding the warping functions of modes 2 and 3 (the bending modes). Then, one solves

$$\left(\mathbf{B}^B - \lambda(\mathbf{B}^B + \mathbf{D}_1^M)\right)\boldsymbol{v} = \mathbf{0}, \tag{17}$$

where the eigenvectors for $0 < \lambda < 1$ define the I shear subspace excluding torsion. The torsional mode is obtained from the $\lambda = 0$ eigenvectors (the nullspace of $\mathbf{B}^B$), by calculating the single non-null eigenvalue of

$$(\mathbf{D}_1^B - \lambda \mathbf{D}_1^M)\boldsymbol{v} = \mathbf{0}, \tag{18}$$

The final deformation modes are normalized as follows: (i) the rigid-body modes correspond to unit displacement/rotations, (ii) the Vlasov, local-plate and I shear modes have a maximum unit in-plane displacement, (iii) the II and III shear modes have a maximum unit warping displacement and (iv) the transverse extension

modes have a maximum unit membrane transverse extension. The proposed procedure was implemented in MATLAB (The MathWorks, 2010). With an Intel Core i7-9700HQ CPU@2.60 GHz processor and an open cross-section with about 20 modes, the runtime is approximately 0.2 seconds. For a closed cross-section with 50 modes, the runtime increases to about 2 seconds.

Figs. 3 and 4 show the deformation modes for two cross-sections, considering $R_C = 0.4$ m and $R_C = 100$ m (Fig. 4c shows only selected modes). In both cases C is taken as the cross-section centroid. It is observed that the mode configurations change with R_C, becoming less symmetric or anti-symmetric as this parameter decreases. Note that, for $R_C = 0.4$, mode 1 does not correspond to uniform warping and mode 3 includes a torsional rotation, as already discussed. Note also that, in Fig. 4b, the center of rotation of mode 4 is slightly offset to the right of the centroid.

4. Numerical Examples

All examples concern 90º cantilevers subjected to end forces, with E = 210 GPa and ν = 0.3. Examples 4.1 to 4.3 are solved using a standard displacement-based GBT FE (see, *e.g.*, Gonçalves & Camotim 2011, 2012), using Hermite cubic and Lagrange quadratic functions, the latter for the deformation modes involving only warping. To prevent locking, 3-point Gauss (reduced) integration along X is used. Along y, 5 Gauss points are employed between cross-section nodes. Along z, analytical integration is carried out due to the $R/R_C \approx 1/\bar{\beta}$ assumption. Finally, example 4.4 compares the performance of the displacement-based element with that of a mixed displacement-strain element, to demonstrate that the latter is particularly efficient for curved members.

The FE procedure was implemented in MATLAB. Although uniform discretizations along X are employed in all cases, the procedure is quite fast – e.g., with an Intel Core i7-9700HQ CPU@2.60 GHz processor, the runtime is below 0.5 seconds for a discretization with 50 elements and 15 deformation modes. For comparison purposes, results obtained with refined 4 node MITC shell FE models, using ADINA (Bathe, 2017), are presented.

4.1 Lipped channel beam subjected to two out-of-plane tip loads

The first example concerns a lipped channel section cantilever subjected to two out-of-plane tip loads, as shown in Fig. 5 (recall also Fig. 3). The GBT cross-section analysis was carried out with 7 nodes, as displayed in the figure.

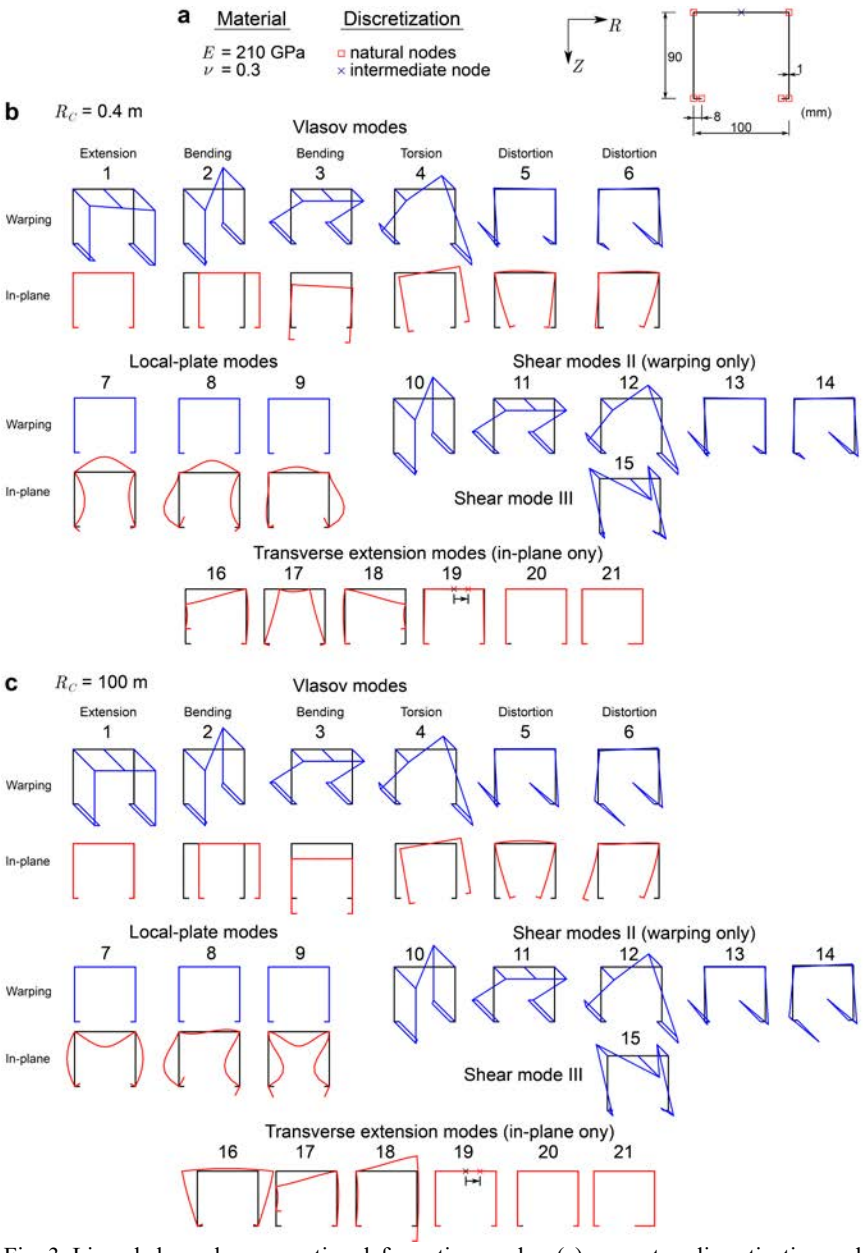

Fig. 3. Lipped channel cross-section deformation modes: (a) geometry, discretization and material parameters, (b) deformation modes for $R_C = 0.4$ m and (c) $R_C = 100$ m.

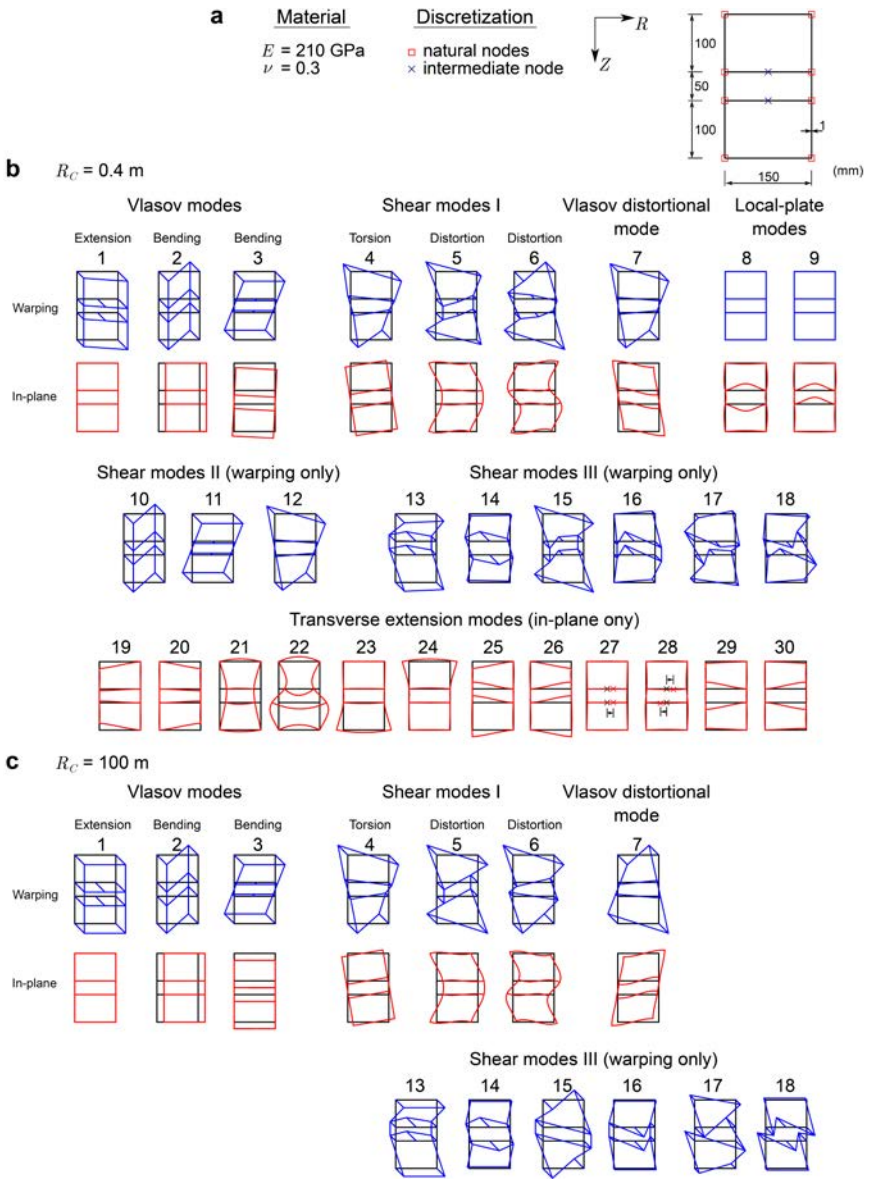

Fig. 4. Three-cell cross-section deformation modes: (a) geometry, discretization and material parameters, (b) deformation modes for $R_C = 0.4$ m and (c) $R_C = 100$ m.

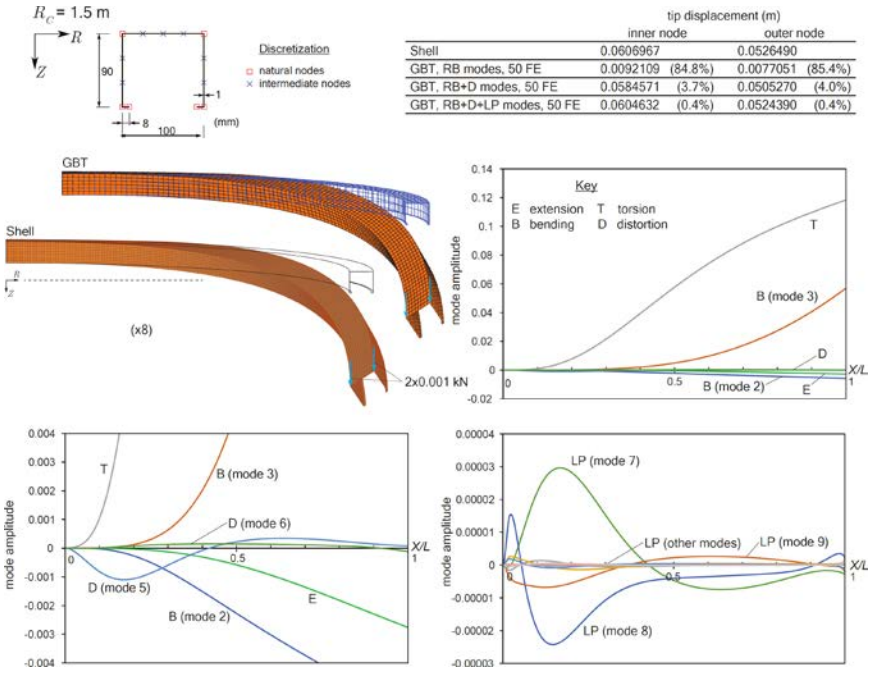

	tip displacement (m) inner node		outer node	
Shell	0.0606967		0.0526490	
GBT, RB modes, 50 FE	0.0092109	(84.8%)	0.0077051	(85.4%)
GBT, RB+D modes, 50 FE	0.0584571	(3.7%)	0.0505270	(4.0%)
GBT, RB+D+LP modes, 50 FE	0.0604632	(0.4%)	0.0524390	(0.4%)

Fig. 5. Lipped channel 90º cantilever subjected to two out-of-plane tip loads.

The table in Fig. 5 shows the tip vertical displacements obtained with a refined shell FE model and the GBT solution, using 50 FEs and different combinations of mode sets: (i) rigid-body (RB), (ii) Vlasov distortional (D) and (iii) local-plate modes (LP) – the shear (S) and transverse extension (TE) modes have a very small influence and therefore were left out. It is concluded that the GBT solution including only the RB modes falls very short of the shell model result. This difference is due to the influence of the D (mostly) and the LP modes, whose inclusion in the analysis leads to results that virtually match those of the shell model, as the deformed configurations displayed in the figure clearly show. This demonstrates that, as in the case of prismatic open sections, only the RB+D+LP modes are normally required to achieve very accurate results.

In spite of the influence of the D and LP modes, they are hardly visible in the deformed configurations. A more in-depth analysis can only be achieved from the mode amplitude graphs in Fig. 5. These graphs show that, although the B and T modes are naturally dominant, the D mode 5 plays a relevant role, namely near the support. The LP modes are only visible in the bottom-right graph, even though their inclusion lowers the displacement error by more than 3 %.

4.2 Three-cell beam subjected to an out-of-plane tip load

A beam with the cross-section of Fig. 4 is analyzed, as shown in Fig. 6. The GBT analyses were carried out with several combinations of mode sets. The table shows that a virtually "exact" GBT solution is obtained when the RB+D+LP modes are included in the analysis. The deformed configurations demonstrate the excellent agreement between the GBT and shell model results: cross-section torsion and distortion are visible throughout the beam and significant local-plate deformation occurs near the fixed end (see the detail in the figure). The mode amplitude graphs confirm these findings: although the RB+D modes are predominant, the LP modes also play a significant role, even if their participations are one order of magnitude below the other ones.

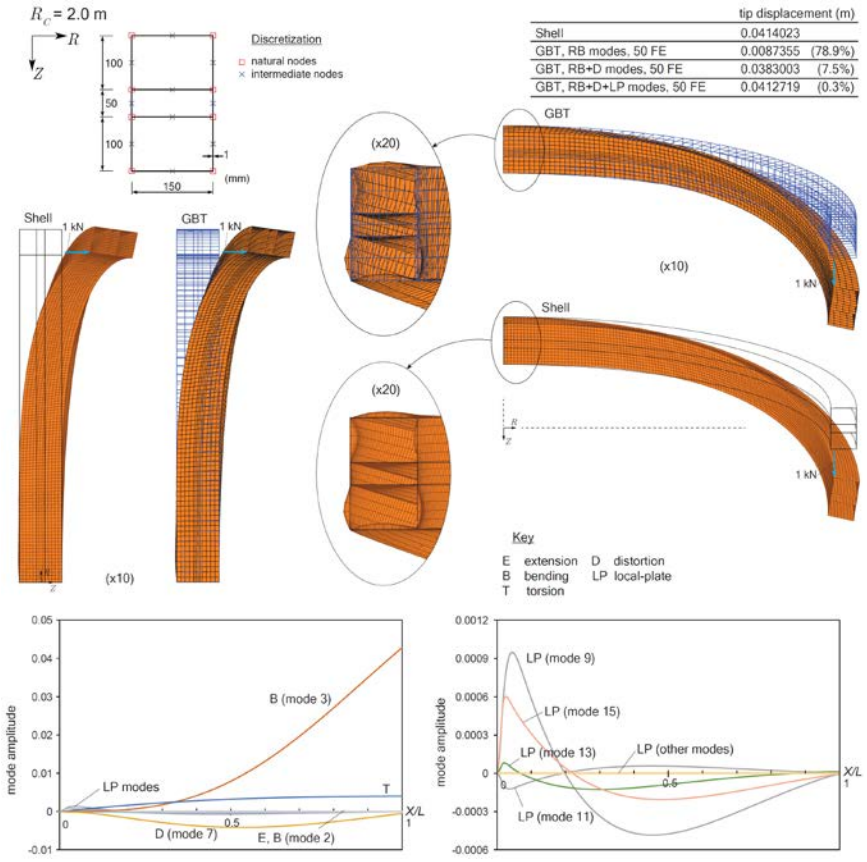

Fig. 6. Three-cell section 90º cantilever subjected to an out-of-plane tip load.

4.3 Twin trapezoidal cell beam subjected to an out-of-plane tip load

This example consists of a twin cell section taken from (Garcea et al., 2016) and shown in Fig. 7, whose discretization leads to 51 deformation modes – the most relevant ones are displayed in the figure.

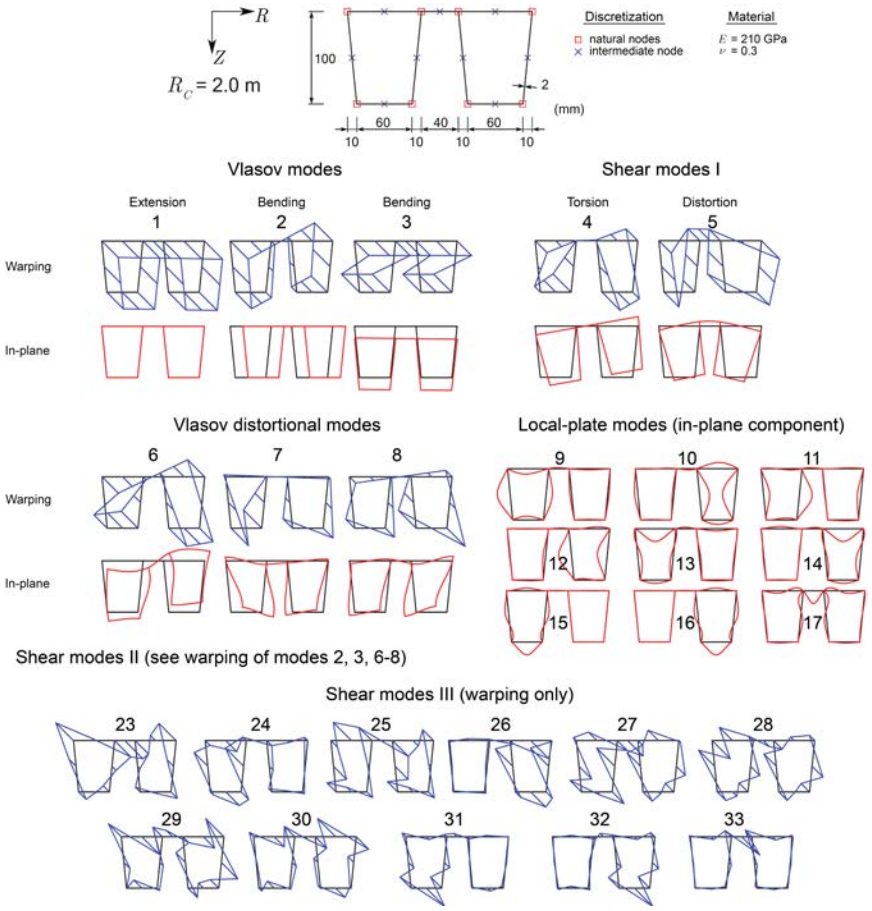

Fig. 7. Twin trapezoidal cell cross-section deformation modes for R_C = 2.0 m.

Fig. 8 shows the results obtained when a single concentrated eccentric vertical force is applied at the free end cross-section of a 90º cantilever. It is once more concluded that the RB modes alone do not provide accurate results. In particular, the three Vlasov D modes (6-8 in Fig. 7) play a significant role. A small

improvement is obtained when either (i) all the LP (9-17) or (ii) the distortional cell shear flow (5) or (iii) all the shear modes are added to the analysis. The deformed configurations clearly demonstrate that there is an excellent match between the shell and GBT models. The bottom-left modal participation graph makes it possible to conclude that the B and T modes are dominant. Nevertheless, the bottom-right graph shows that all three Vlasov D modes are also quite relevant throughout the beam length, followed by the cell shear flow mode 5. The LP modes are only important near the fixed end.

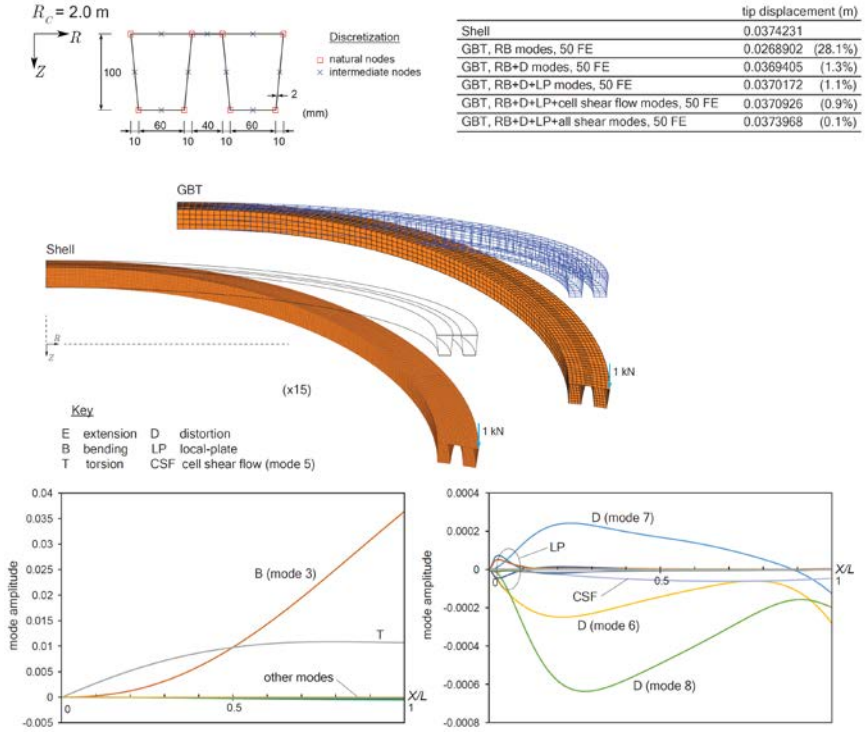

	tip displacement (m)	
Shell	0.0374231	
GBT, RB modes, 50 FE	0.0268902	(28.1%)
GBT, RB+D modes, 50 FE	0.0369405	(1.3%)
GBT, RB+D+LP modes, 50 FE	0.0370172	(1.1%)
GBT, RB+D+LP+cell shear flow modes, 50 FE	0.0370926	(0.9%)
GBT, RB+D+LP+all shear modes, 50 FE	0.0373968	(0.1%)

Fig. 8. Twin trapezoidal cell section 90º cantilever subjected to an out-of-plane tip load.

4.4 Comparison between compatibility and mixed elements

In this example, the displacement-based FE is compared with a mixed strain-displacement FE. The latter is obtained using the Hellinger-Reissner principle and approximating the strains associated with each deformation mode using linear functions. The additional DOFs are subsequently eliminated at the element level.

Fig. 9 compares the performance of the two GBT-based FE with the classic Winkler solution, for a 90º cantilever subjected to a tip load. It is observed that the displacement-based FE requires 10 elements to achieve accurate results, whereas the mixed element leads to good results with just one or two elements.

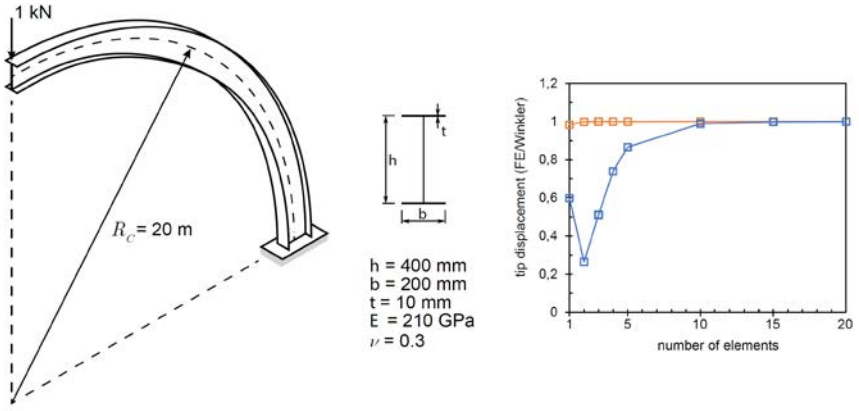

Fig. 9. I-section 90º cantilever subjected to an in-plane tip load.

5. Concluding Remarks

This paper improved the first-order GBT formulation for curved thin-walled members introduced by Peres et al. (2016) by presenting a systematic procedure to obtain the cross-section deformation modes for arbitrary flat-walled cross-sections (open, closed or "mixed"). This procedure retains the nomenclature of the deformation mode subsets defined for prismatic members, by handling adequately the complex kinematics pertaining to curved bars. In particular, it was shown that (i) very accurate solutions are generally obtained with only a small set of modes and (ii) the modal features of the GBT solution can provide in-depth insight into the structural behavior of naturally curved bars. Finally, it was shown that a mixed strain-displacement FE format is much more accurate than its displacement-based format. This mixed element is currently being developed to include all deformation modes. The results will be presented in the near future.

Acknowledgements

The first author gratefully acknowledges the financial support of FCT (Fundação para a Ciência e a Tecnologia, Portugal), through the doctoral scholarship SFRH/BD/120062/2016.

References

Bathe KJ, *ADINA System*, ADINA R&D Inc, 2017.

Bebiano R, Gonçalves R, Camotim D (2015). A cross-section analysis procedure to rationalise and automate the performance of GBT-based structural analyses, *Thin-Walled Structures*, 92, 29-47.

Camotim D, Basaglia C, Bebiano R, Gonçalves R, Silvestre N (2010a). Latest developments in the GBT analysis of thin-walled steel structures. *Proc. of Int. Col. Stability and Ductility of Steel Structures*, E. Batista et al. (eds.), 33-58.

Camotim, D, Basaglia C, Silva N, Silvestre N (2010b). Numerical analysis of thin-walled structures using generalised beam theory (GBT): Recent and future developments. *Computational Technology Reviews,* B. Topping et al. (eds.), Saxe-Coburg, 315-354.

Dabrowski R (1968). Gekrümmte dünnwandige Träger. Theorie und Berechnung, Springer-Verlag, Berlin/Heidelberg/New York.

Garcea G, Gonçalves R, Bilotta A, Manta D, Bebiano R, Leonetti L, Magisano D, Camotim D (2016). Deformation modes of thin-walled members: A comparison between the method of Generalized Eigenvectors and Generalized Beam Theory, *Thin-Walled Structures*, 100, 192-212.

Gonçalves R, Camotim D (2011). Generalised Beam Theory-based finite elements for elastoplastic thin-walled metal members, *Thin-Walled Structures*, 49(10), 1237-1245.

Gonçalves R, Camotim D (2012). Geometrically non-linear Generalised Beam Theory for elastoplastic thin-walled metal members, *Thin-Walled Structures*, 51(February), 121-129.

Gonçalves R, Ritto-Corrêa M, Camotim D (2010). A new approach to the calculation of cross-section deformation modes in the framework of Generalized Beam Theory, *Computational Mechanics*, 46(5), 759-781.

Gonçalves R, Bebiano R, Camotim D (2014). On the shear deformation modes in the framework of Generalized Beam Theory, *Thin-Walled Structures*, 84, 325-334.

MATLAB, version 7.10.0 (R2010a), The MathWorks Inc., Massachusetts, 2010.

Peres N, Gonçalves R, Camotim D (2016). First-order Generalised Beam Theory for curved thin-walled members with circular axis, *Thin-Walled Structures*, 107, 345-361.

Schardt R (1966), Eine erweiterung der technischen biegetheorie zur berechnung prismatischer faltwerke, *Stahlbau*, 35, 161–171. (German)

Schardt R (1989). *Verallgemeinerte Technische Biegetheorie*, Springer Verlag, Berlin. (German)

The MathWorks Inc. (2010). *MATLAB Version 7.10.0* (*R2010a*).

Vlasov V (1958). *Tonkostenye Sterjni*, Fizmatgiz, Moscow. (Russian)

Winkler E (1868). *Die Lehre von der Elasticitaet und Festigkeit*, H. Dominicus, Prague. (German)